Facile Synthesis and Characterization of Novel Mesoporous and Mesorelief Oxides with Gyroidal Structures

ARTICLE *in* JOURNAL OF THE AMERICAN CHEMICAL SOCIETY · FEBRUARY 2004

Impact Factor: 12.11 · DOI: 10.1021/ja037877t · Source: PubMed

12 AUTHORS, INCLUDING:

Bozhi Tian
University of Chicago
91 PUBLICATIONS **7,391** CITATIONS
SEE PROFILE

Zhendong Zhang
The Chinese University of Hong Kong
14 PUBLICATIONS **660** CITATIONS
SEE PROFILE

Osamu Terasaki
Stockholm University
437 PUBLICATIONS **20,854** CITATIONS
SEE PROFILE

Dongyuan Zhao
Monash University (Australia)
524 PUBLICATIONS **26,690** CITATIONS
SEE PROFILE

J|A|C|S
ARTICLES
Published on Web 12/30/2003

Facile Synthesis and Characterization of Novel Mesoporous and Mesorelief Oxides with Gyroidal Structures

Bozhi Tian,[†] Xiaoying Liu,[†] Leonid A. Solovyov,[‡] Zheng Liu,[§] Haifeng Yang,[†] Zhendong Zhang,[†] Songhai Xie,[†] Fuqiang Zhang,[†] Bo Tu,[†] Chengzhong Yu,[†] Osamu Terasaki,[||] and Dongyuan Zhao*,[†]

Contribution from the Molecular Catalysis and Innovative Materials Lab, Department of Chemistry, Fudan University, Shanghai 200433, P. R. China, Institute of Chemistry and Chemical Technology, 660049 Krasnoyarsk, Russia, Bio Nanotec Research Institute (BNRI), Sendai 980-8578, Japan, and Structural Chemistry, Arrhenius Laboratory, Stockholm University, S-106 91 Stockholm, Sweden

Received August 12, 2003; E-mail: dyzhao@fudan.edu.cn

Abstract: In this paper, we bring forward an effective strategy, solvothermal postsynthesis, to prepare ordered mesoporous silica materials with highly branched channels. Structural characterizations indicate that the titled mesoporous materials basically have the cubic double gyroidal (space group *Ia*-3*d*) structure with small fraction of distortions. The mesopore sizes and surface areas can be up to 8.8 nm and 540 m^2/g, respectively, when microwave digestion is employed to remove the organic templates. A phase transition model is proposed, and possible explanations for the successful phase transition are elucidated. The results show that the flexible inorganic framework, high content of organic matrix, and nonpenetration of poly(ethylene oxide) segments may facilitate the structural evolution. This new synthetic strategy can also be extended to the preparation of other double gyroidal silica-based mesoporous materials, such as metal and nonmetal ions doped silica and organo-functionalized silica materials. The prepared 3D mesoporous silica can be further utilized to fabricate various ordered crystalline gyroidal metal oxide "negatives". The mesorelief "negatives" (Co_3O_4 and In_2O_3 are detailed here) prepared by impregnation and thermolysis procedures exhibit undisplaced, displaced, and uncoupled enantiomeric gyroidal sub-frameworks. It has been found that the amount of metal oxide precursors (hydrated metal nitrates) greatly influence the (sub)framework structure and single crystallinity of the mesorelief metal oxide particles. The single crystalline gyroidal metal oxides are ordered both at mesoscale and atomic scale. However, these orders are not commensurate with each other.

Introduction

The organization and assembly of inorganic and organic materials into a wealth of textured forms represent an exciting direction for developing novel multifunctional materials.[1] Mesoporous materials [2] prepared via "soft chemistry" (templated by surfactants, block copolymers, colloids, etc.) have overcome the restriction of the dimensions and accessibility of the well-developed microporous solids and, therefore, have sparked a wide spectrum of interests in areas such as catalysis, chemical and biological separation, photonic and electronic devices, and drug delivery.[3−5] Among the known mesostructured forms, the cubic bicontinuous structure (space group, *Ia*-3*d*, represented by MCM-48) may be the most complex one[6] that has attracted much attention and would show fantastic properties. The mesoscopic surface of MCM-48 material is defined by a so-

[†] Fudan University.
[‡] Institute of Chemistry and Chemical Technology.
[§] BNRI.
[||] Stockholm University.

(1) (a) Soler-illia, G. J. D. A.; Sanchez, C.; Lebeau, B.; Patarin, J. *Chem. Rev.* **2002**, *102*, 4093. (b) Sanchez, C.; Soler-Illia G. J. D. A.; Ribot, F.; Lalot, T.; Mayer, C. R.; Cabuil, V. *Chem. Mater.* **2001**, *13*, 3061. (c) Sayari, A.; Hamoudi, S. *Chem. Mater.* **2001**, *13*, 3151. (d) Walcarius, A. *Chem. Mater.* **2001**, *13*, 3351. (e) Chaumel, F.; Jiang, H. W.; Kakkar, A. *Chem. Mater.* **2001**, *13*, 3389. (f) Lacroix, P. G. *Chem. Mater.* **2001**, *13*, 3495. (g) Forster, S.; Plantenberg, T. *Angew. Chem., Int. Ed.* **2002**, *41*, 689. (h) Corriu, R. J. P. *Eur. J. Inorg. Chem.* **2001**, 1109. (i) Chujo, Y. *Curr. Opin. Solid State Mater. Sci.* **1996**, *1*, 806. (j) Stein, A.; Melde, B. J.; Schroden, R. C. *Adv. Mater.* **2000**, *19*, 1304.

(2) (a) Liebau, F. *Microporous Mesoporous Mater.* **2003**, *58*, 15. (b) Schuth, F.; Schmidt, W. *Adv. Mater.* **2002**, *14*, 629. (c) Schuth, F. *Chem. Mater.* **2001**, *13*, 3184. (d) Stein, A. *Adv. Mater.* **2003**, *15*, 763.

(3) (a) Ying, J. Y.; Mehnert, C. P.; Wong, M. S. *Angew. Chem., Int. Ed.* **1999**, *38*, 56. (b) Corma, A. *Top. Catal.* **1997**, *4*, 249. (c) Scott, B. J.; Wirnsberger, G.; Stucky, G. D. *Chem. Mater.* **2001**, *13*, 3140. (d) He, X.; Antonelli, D. *Angew. Chem, Int. Ed.* **2001**, *41*, 214.

(4) (a) Mal, N. K.; Fujiwara, M.; Tanaka, Y. *Nature* **2003**, *421*, 350. (b) Lai, C. Y.; Trewyn, B. G.; Jeftinija, D. M.; Jeftinija, K.; Xu, S.; Jeftinija, S.; Lin, V. S. Y. *J. Am. Chem. Soc.* **2003**, *125*, 4451. (c) Munoz, B.; Ramila, A.; Perez-Pariente, J.; Diaz, I.; Vallet-Regi, M. *Chem. Mater.* **2003**, *15*, 500.

(5) (a) Newalkar, B. L.; Choudary, N. V.; Turaga, U. T.; Vijayalakshmi, R. P.; Kumar, P.; Komarneni, S.; Bhat, T. S. G. *Chem. Mater.* **2003**, *15*, 1474. (b) Zhao, J.; Gao, F.; Fu, Y.; Jin, W.; Yang, P.; Zhao, D. *Chem. Commun.* **2002**, 752. (c) Han, Y. J.; Stucky, G. D.; Butler, A. *J. Am. Chem. Soc.* **1999**, *121*, 9897. (d) Dai, S.; Burleigh, M. C.; Ju, Y. H.; Gao, H. J.; Lin, J. S.; Pennycook, S. J.; Barnes, C. E.; Xue, Z. L. *J. Am. Chem. Soc.* **2000**, *122*, 992.

(6) (a) Andersson, S.; Hyde, S. T.; Larsson, K.; Lidin, S. *Chem. Rev.* **1988**, *88*, 221. (b) Alfredsson, V.; Anderson, M. W. *Chem. Mater.* **1996**, *8*, 1141. (c) Hyde, S. T. *Curr. Opin. Solid State Mater. Sci.* **1996**, *1*, 653. (d) Fontell, K. *Colloid Polym. Sci.* **1990**, *268*, 264. (e) Auvray, X.; Petipas, C.; Anthore, R.; Rico, I.; Lattes, A. J. *J. Phys. Chem.* **1989**, *93*, 7458. (f) Gier, T. E.; Bu, X.; Stucky, G. D. *Nature* **1998**, *395*, 154.

called minimal surface, gyroid (G-surface), which is also observed in water−lipid or water−surfactant systems[6d,e] and artifical zeolite-like open frameworks.[6f] In general, the double gyroidal mesostructure has a unique three-dimensional (3D) network with channels running along ⟨100⟩ and ⟨111⟩ directions, making the pore system available in three dimensions.[7] Therefore, it paves the much more direct and easier inclusion of various "guest" elements into the cavum of the "host" matrix compared with other mesostructured materials. However, the conventional MCM-48 material shows a relatively small pore size (usually no more than 4 nm) and must be synthesized under a basic medium by using cationic surfactants as templates,[8] which may dampen the possibility to introduce the large molecules or the utilization of the channels for the fabrication of architectural nano-objects.

Until now, only a few published works have documented the synthesis of large-pore (above 5 nm) double gyroidal mesoporous solids templated by block copolymers.[9−11] The basic strategies used for the preparation of such bicontinuous materials include the strict selection of proper organic templates,[9] the employment of some additives such as 3-mercaptopropyltrimethoxysilane (MPTS), butanol, and inorganic salts,[10] and the control of organic template concentration and solvent evaporation behavior.[11] A simple, low-cost, reproducible synthesis and easier control are desired to facilitate the formation of the aforementioned mesostructured solids.

Porous crystals, especially the ordered porous single crystals, are hierarchically ordered at different length scales, e.g., the macro-/atomic scales, the meso-/atomic scales, and the macro-/meso-/atomic scales. These materials have long been the focus in research areas such as biomineralization and inorganic materials.[12] Besides the marvelous organizations and morphologies, the great interest in these hierarchical porous crystals also lies in their novel physicochemical properties and specific crystallography. The natural or synthetic forms of the porous single crystals always derive from the controlled deposition of minerals on the organic matrixes or molds exerted by the organic (soft) matter.[12] An alternative strategy to fabricate porous crystals is via the hard templating pathway, i.e., "guest" materials faithfully copy the "inverse" or "surface" structures of the "host" inorganic materials. Hard template for the preparation of ordered nanostructures has some advantages compared with soft template, especially in its specific topological stability, veracity, predictability, and controllability. The hard template (e.g., alumina membranes, latex spheres, carbon nanotubes) has been extensively used for the production of nanowires and other related nanoreplicas.[13−15] However, all these hard templates cannot produce complex forms (such as gyroid structure, *Ia*-3*d*) of "guest" materials, for example, electrochemical etched alumina membranes can only fabricate 1D nanowires, nanorods, or nanotubes; latex spheres usually adopt a hexagonal close-packed or cubic close-packed lattice, which also limits the variety of "negative" morphologies. Furthermore, the single crystallinity of the crystals prepared by these templates is always far from desired. Mesoporous materials, a class of new and attractive candidates as the hard templates, have already displayed their power to fabricate a great variety of nanostructured composites,[16−19] such as carbon,[16] metal,[17] semiconductor,[18] and oxides.[19] Moreover, the rich topological varieties of mesoporous "hosts" lead to the architectural abundance of the replicated "guest" materials.

In this paper, we demonstrate for the first time a simple solvothermal post-treatment method to prepare ordered large-pore (>7 nm) mesoporous silica with double gyroidal channels via phase transition from 2D hexagonal mesophase. This new synthetic strategy of solvothermal post-treatment can be simply performed in many organic solvents such as *n*-hexane at ∼60−100 °C, and be extended to the syntheses of other double gyroidal silica-based mesoporous materials, such as metal and nonmetal ions doped silica and organo-functionalized silica materials. And to make it further, we employ this mesostructured silica product as the "hard template" to fabricate various porous metal oxide crystals with the similar gyroidal (sub)frameworks.

(7) (a) Anderson, M. W. *Zeolites* **1997**, *19*, 220. (b) Alfredsson, V.; Anderson, M. W.; Ohsuna, T.; Terasaki, O.; Jacob, M.; Bojrup, M. *Chem. Mater.* **1997**, *9*, 2066. (c) Kaneda, M.; Tsubakiyama, T.; Carlsson, A.; Sakamoto, Y.; Ohsuna, T.; Terasaki, O.; Joo, S. H.; Ryoo, R. *J. Phys. Chem. B* **2002**, *106*, 1256.

(8) (a) Beck, J. S.; Vartuli, J. C.; Roth, W. J.; Leonowicz, M. E.; Kresge, C. T.; Schmitt, K. D.; Chu, C. T. W.; Olson, D. H.; Sheppard, E. W.; Mccullen, S. B.; Higgins, J. B.; Schlenker, J. L. *J. Am. Chem. Soc.* **1992**, *114*, 10834. (b) Huo, Q. S.; Margolese, D. I.; Stucky, G. D. *Chem. Mater.* **1996**, *8*, 1147.

(9) (a) Chan, V. Z. H.; Hoffman, J.; Lee, V. Y.; Iatrou, H.; Avgeropoulos, A.; Hadjichristidis, N.; Miller, R. D.; Thomas, E. L. *Science* **1999**, *286*, 1716. (b) Chan, Y. T.; Lin, H. P.; Mou, C. Y.; Liu, S. T. *Chem. Commun.* **2002**, 2878.

(10) (a) Liu, X.; Tian, B.; Yu, C.; Gao, F.; Xie, S.; Tu, B.; Che, R.; Peng, L. M.; Zhao, D. *Angew. Chem., Int. Ed.* **2002**, *41*, 3876. (b) Kleitz, F.; Choi, S. H.; Ryoo, R. *Chem. Commun.* **2003**, 2136. (c) Flodstrom, K.; Alfredsson, V.; Kallrot, N. *J. Am. Chem. Soc.* **2003**, *125*, 4402.

(11) (a) Tian, B.; Liu, X.; Tu, B.; Yu, C.; Fan, J.; Wang, L.; Xie, S.; Stucky, G. D.; Zhao, D. *Nat. Mater.* **2003**, *2*, 159. (b) Yang, H.; Shi, Q.; Liu, X.; Xie, S.; Jiang, D.; Zhang, F.; Yu, C.; Tu, B.; Zhao, D. *Chem. Commun.* **2002**, 2842.

(12) (a) Mann, S. *Angew. Chem., Int. Ed.* **2000**, *39*, 3393. (b) Mann, S. *Nature* **1993**, *365*, 499. (c) Aizenberg, J.; Hanson, J.; Koetzle, T. F.; Weiner, S.; Addadi, L. *J. Am. Chem. Soc.* **1997**, *119*, 881. (d) Zhan, J. H.; Lin, H. P.; Mou, C. Y. *Adv. Mater.* **2003**, *15*, 621. (e) Mann, S. *Biomineralization: Principles and Concepts in Bioinorganic Materials Chemistry*; Oxford University Press: New York, 2001.

(13) (a) Martin, C. R.; Mitchell, D. T. *Electroanal. Chem.* **1999**, *21*, 1. (b) Schmid, G.; Baumle, M.; Geerkens, M.; Heim, I.; Osemann, C.; Sawitowski, T. *Chem. Soc. Rev.* **1999**, *28*, 179. (c) Lei, Y.; Zhang, L.; Meng, G.; Li, G.; Zhang, X.; Liang, C.; Chen, W.; Wang, S. *Appl. Phys. Lett.* **2001**, *78*, 1125. (d) Sun, L.; Searson, P. C.; Chien, C. L. *Appl. Phys. Lett.* **1999**, *74*, 2803.

(14) (a) Stein, A.; Schroden, R. C. *Curr. Opin. Solid State Mater. Sci.* **2001**, *5*, 553. (b) Xia, Y.; Gates, B.; Yin, Y.; Lu, Y. *Adv. Mater.* **2000**, *12*, 693. (c) *Adv. Mater.* **2001**, *13* (6) (special issue on photonic crystals and most articles therein).

(15) (a) Dai, H.; Wong, E.; Lu, Y.; Fan, S.; Lieber, C. M. *Nature* **1995**, *375*, 769. (b) Govindaraj, A.; Satishkumar, B. C.; Nath, M.; Rao, C. N. R. *Chem. Mater.* **2000**, *12*, 202. (c) Sloan, J.; Wright, D. M.; Woo, H.-G.; Bailey, S.; York, A. P. E.; Coleman, K. S.; Hutchison, J. L.; Green, M. L. H. *Chem. Commun.* **1999**, 699.

(16) (a) Ryoo, R.; Joo, S. H.; Jun, S. *J. Phys. Chem. B* **1999**, *103*, 7745. (b) Lee, J.; Yoon, S.; Hyeon, T.; Oh, S. M.; Kim, K. B. *Chem. Commun.* **1999**, 2177. (c) Tian, B.; Che, S.; Liu, Z.; Liu, X.; Fan, W.; Tatsumi, T.; Terasaki, O.; Zhao, D. *Chem. Commun.* **2003**, 2726.

(17) (a) Shin, H. J.; Ryoo, R.; Liu, Z. Terasaki, O. *J. Am. Chem. Soc.* **2001**, *123*, 1246. (b) Ko, C. H.; Ryoo, R. *Chem. Commun.* **1996**, 2467. (c) Liu, Z.; Sakamoto, Y.; Ohsuna, T.; Hiraga, K.; Terasaki, O.; Ko, C. H.; Shin, H. J.; Ryoo, R. *Angew. Chem., Int. Ed.* **2000**, *39*, 3107. (d) Han, Y.-J.; Kim, J. M.; Stucky, G. D. *Chem. Mater.* **2000**, *12*, 2068. (e) Huang, M. H.; Choudrey, A.; Yang, P. *Chem. Commun.* **2000**, 1063. (f) Plyuto, Y.; Berquier, J. M.; Jacquoid, C.; Ricolleau, C. *Chem. Commun.* **1999**, 1653. (g) Fukuoka, A.; Sakamoto, Y.; Guan, S.; Inagaki, S.; Sugimoto, N.; Fukushima, Y.; Hirahara, K.; Iijima, S.; Ichikawa, M. *J. Am. Chem. Soc.* **2001**, *123*, 3373. (h) Kang, H.; Jun, Y.-W.; Park, J.-I.; Lee, K.-B.; Cheon, J. *Chem. Mater.* **2000**, *12*, 3530. (i) Zhang, Z.; Dai, S.; Blom, D. A.; Shen, J. *Chem. Mater.* **2002**, *14*, 965.

(18) (a) Coleman, N. R. B.; Morris, M. A.; Spalding, T. R.; Holmes, J. D. *J. Am. Chem. Soc.* **2001**, *123*, 187. (b) Coleman, N. R. B.; O'Sullivan, N.; Ryan, K. M.; Crowley, T. A.; Morris, M. A.; Spalding, T. R.; Steytler, D. C.; Holmes, J. D. *J. Am. Chem. Soc.* **2001**, *123*, 7010. (c) Ryan, K. M.; Erts, D.; Olin, H.; Morris, M. A.; Holmes, J. D. *J. Am. Chem. Soc.* **2003**, *125*, 6284. (d) Gao, F.; Lu, Q.; Zhao, D. *Adv. Mater.* **2003**, *15*, 739.

(19) (a) Zhu, K.; Yue, B.; Zhou, W.; He, H. *Chem. Commun.* **2003**, 98. (b) Yang, H.; Shi, Q.; Tian, B.; Lu, Q.; Gao, F.; Xie, S.; Fan, J.; Yu, C.; Tu, B.; Zhao, D. *J. Am. Chem. Soc.* **2003**, *125*, 4672. (c) Tian, B.; Liu, X.; Yang, H.; Xie, S.; Yu, C.; Tu B.; Zhao, D. *Adv. Mater.* **2003**, 15, 1370. (d) Laha, S. C.; Ryoo, R. *Chem. Commun.* **2003**, 2138.

A large number of the mesorelief "negatives" such as Co_3O_4 and In_2O_3 have been prepared via impregnation and thermolysis procedures. These ordered metal oxide mesoreliefs have large surface areas (generally larger than 70 m^2/g) and exhibit single crystallinity in domains.

Experimental Section

Chemicals. Triblock poly(ethylene oxide)-*b*-poly(propylene oxide)-*b*-poly(ethylene oxide) copolymer Pluronic P123 (Mw = 5800, EO_{20}-$PO_{70}EO_{20}$) and (3-chloropropyl)trimethoxysilane (CPTMS, 98%) were purchased from Aldrich Co. and Acros Co., respectively. Other chemicals were purchased from Shanghai Chemical Co. All chemicals were used as received. Millipore water was used in all experiments.

Preparation. A general procedure was as follows: The as-made mesostructured silica "precursor" membranes (sample S5) templated by triblock copolymer Pluronic P123 were prepared by the evaporation-induced self-assembly (EISA) process.[20a] Then the as-made hybrid precursors were collected and sealed within a Teflon bottle containing 70% capacity of *n*-hexane. Solvothermal treatment at 80 °C for 3 days was conducted before the products were filtered, calcined (sample S2), or microwave digested (sample S3).[21] The as-made hybrid membranes were also directly calcined to get the hollowed out forms (sample S1). For comparison, as-made (without hydrothermal treatment) SBA-15 powder (sample S4) prepared as described in a previous paper[20b] also conducted the aforementioned solvothermal post-treatment. The metal oxide replicas were prepared by two-step impregnation and thermolysis procedures and using S3 as a hard template. Generally, 0.15 g of S3 was impregnated with ~1.8−2.6 mmol of hydrated metal nitrates in total (sample C1/2.0 mmol of $Co(NO_3)_2{\cdot}6H_2O$, C2/2.6 mmol of $Co(NO_3)_2{\cdot}6H_2O$, sample I1/1.8 mmol of $In(NO_3)_3{\cdot}4.5H_2O$, I2/2.2 mmol of $In(NO_3)_3{\cdot}4.5H_2O$). Commercial In_2O_3 powder (sample I3) was used to compare and illustrate the optic properties of titled In_2O_3 nanostructured materials (see details in the Supporting Information).

Various metal (nonmetal) ions doped or organo-functionalized gyroidal mesoporous silica materials were prepared according to similar procedures, except that the membrane "precursors" were 2D hexagonal ion doped or organo-functionalized hybrid materials. The ion dopants could be Ti, Al, W, Nb, Mn, B, etc., and the functional groups could be 3-aminopropyl-, 3-chloropropyl-, 3-mercaptopropyl-, pheyl-, etc.

Characterization. The structural quality was monitored by low-angle X-ray diffraction (XRD), recorded on a German Bruker D4 X-ray diffractometer with Ni-filtered Cu Kα radiation. Transmission electron microscopy (TEM) experiments were conducted on a JEOL 2011 microscope operated at 200 kV or on a JEM-4000EX microscope operated at 400 kV. Scanning electron microscopy (SEM) images were obtained on Philip XL30 operated at 20 kV. Ultraviolet diffuse reflectance spectra (UV−DRS) were obtained with JASCO V-550 UV−vis spectrometer equipped with integrating sphere attachment. Solid-state ^{29}Si NMR experiments were performed on a Bruker DSX300 spectrometer with a frequency of 59.63 MHz, a recycling delay of 600 s, and a radiation frequency intensity of 62.5 kHz. The thermal decomposition behaviors of the products were monitored using Mettler Toledo TGA/SDTA851 over the temperature range of ~25−900 °C, with a heating rate of 5 °C/min. Photoluminescence (PL) spectra were collected on F-4500 FL spectrophotometer, with the excitation wavelength of 270 nm. Nitrogen adsorption/desorption isotherms were measured at 77 K on a nitrogen adsorption apparatus (Quantachrome Autosorb-1 Adsorption apparatus) after degassing samples at 180 °C for 5 h. The Brunauer−Emmett−Teller (BET) surface area (S_{BET}) was estimated using adsorption data in a relative pressure range from 0.04 to 0.3. The total pore volume, V_t, was estimated from the amount adsorbed at a relative pressure of 0.95. The micropore volume, V_{mi}, and micropore area, S_{mi}, were calculated using the *t*-plot method (thickness range: 0.29−0.46 nm). The mesopore size distributions (PSD) were calculated by analyzing the adsorption data of the N_2 isotherm using the Barrett−Joyner−Halenda (BJH) method.

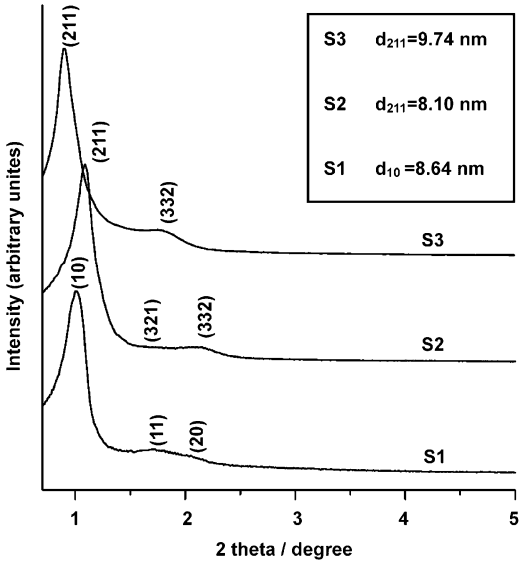

Figure 1. Small-angle X-ray diffraction patterns of (S1) calcined 2D hexagonal, (S2) calcined, and (S3) digested 3D bicontinuous cubic mesoporous silica materials prepared from EISA.

Modeling and Simulation. The structure modeling of the crystalline metal oxide replicas was carried out using the density distribution function[22a] developed for Gyroid mesostructures and applied previously to CMK-1 carbon[22a] and MCM-48 silica[22a,b] mesostructured materials. This function allowed density distribution simulation for different porous, composite, and framework materials with structural elements following the Gyroid surface[22c] topology. The TEM simulations were performed by projecting the density distribution function on respective crystallographic planes.

Results and Discussion

1. Silica-Based Mesoporous Materials. Figure 1 shows the powder XRD patterns of mesoporous silica products. Calcined sample S1 prepared by EISA procedure and without the solvothermal post-treatment is typical of the well-ordered 2D hexagonal mesostructure (space group, *p*6*mm*), which is characterized by the 10, 11, and 20 reflections. The Bragg diffraction peaks are relatively broader than those for mesoporous SBA-15 powders, probably due to the uniaxial structural distortion (contraction) that is always observed for the mesostructured materials prepared via the EISA process.[23] TEM images (not shown here) further show that S1 has a well-ordered

(20) (a) Zhao, D.; Yang, P.; Melosh, N.; Feng, J.; Chmelka, B. F.; Stucky, G. D. *Adv. Mater.* **1998**, *10*, 1380. (b) Zhao, D.; Feng, J.; Huo, Q.; Melosh, N.; Fredrickson, G. H.; Chmelka, B. F.; Stucky, G. D. *Science* **1998**, *279*, 548.

(21) Tian, B.; Liu, X.; Yu, C.; Gao, F.; Luo, Q.; Xie, S.; Tu, B.; Zhao, D. *Chem. Commun.* **2002**, 1186.

(22) (a) Solovyov, L. A.; Zaikovskii, V. I.; Shmakov, A. N.; Belousov, O. V.; Ryoo, R. *J. Phys. Chem. B* **2002**, *106*, 12198. (b) Solovyov, L. A.; Belousov, O. V.; Shmakov, A. N.; Zaikovskii, V. I.; Joo, S. H.; Ryoo, R.; Haddad, E.; Gedeon A.; Kirik. S. D. *Stud. Surf. Sci. Catal.* **2003**, *146*, 299. (c) Schoen, A. H. NASA Technical Note D-5541; NASA: Washington, DC, 1970.

(23) (a) Klotz, M.; Albouy, P.-A.; Ayral, A.; Ménager, C.; Grosso, D.; Lee, A. V.; Cabuil, V.; Babonneau, F.; Guizard, C. *Chem. Mater.* **2000**, *12*, 1721. (b) Grosso, D.; Balkenende, A. R.; Albouy, P. A.; Ayral, A.; Amenitsch, H.; Babonneau, F. *Chem. Mater.* **2001**, *13*, 1848. (c) Grosso, D.; Soler-Illia, G. J. D. A. A.; Babonneau, F.; Sanchez, C.; Albouy, P. A.; Brunet-Bruneau, A.; Balkenende, A. R. *Adv. Mater.* **2001**, *13*, 1085. (d) Crepaldi, E.; Soler-Illia, G. J. D. A.; Bouchara, A.; Grosso, D.; Durand, D.; Sanchez, C. *Angew. Chem., Int. Ed.* **2003**, *42*, 374. (e) Hillhouse, H. W.; van Egmond, J. W.; Tsapatsis, M.; Hanson, J. C.; Larese, J. Z. *Chem. Mater.* **2000**, *12*, 2888.

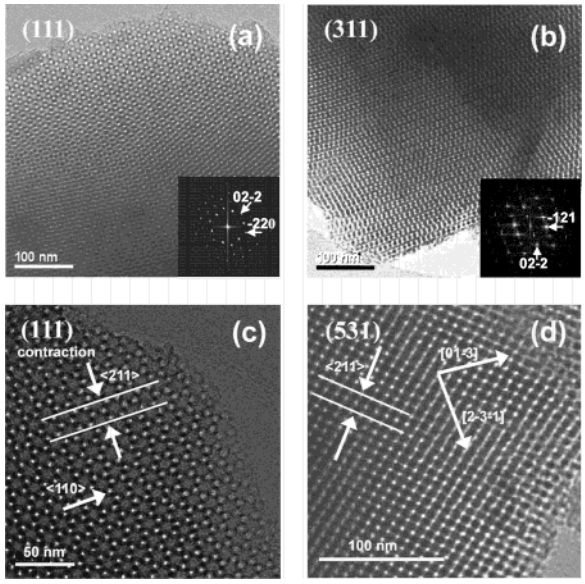

Figure 2. TEM images of calcined gyroidal mesoporous silica (S2), along (a) [111] and (b) [311] zone axes; insets are corresponding FDs. (c) and (d) Distorted (111) and (531) projection planes.

2D hexagonal mesostructure. After the solvothermal post-treatment (S2 and S3), XRD patterns (Figure 1) show that the diffraction peaks change dramatically in positions and intensities, suggesting a mesophase transition. Combined with the TEM results (discussed below), we tentatively consider the possible space group *Ia*-3*d* for the transformed mesostructure. Accordingly, we assigned the diffraction peaks corresponding to the *Ia*-3*d* mesophase, i.e., 211, 321, and 332. The poorly resolved peaks of the solvothermal-treated samples clearly resulted from the partially distorted mesostructured membrane "precursors". Combined with previous literature,[24a] the 211 reflections of samples S2 and S3 (calcined and microwave-digested silica materials after the solvothermal post-treatment, respectively) may evolve from the 10 reflection of S1, due to a possible geometrical correlation between those two planes. Meanwhile, the d_{211} spacing of S3 is 9.74 nm, larger than that of S2 (8.10 nm), clearly suggesting that the calcination causes much greater structural shrinkage than the microwave digestion upon the removal of organic templates.[21] The d_{211} spacing of S2 is a little smaller than the d_{10} spacing of S1 (8.64 nm), in accord with previous in situ XRD results[24a] where a decrease in *d*-spacing was observed when MCM-41 was transformed to MCM-48. The cell parameter, *a*, is calculated to be 9.98, 19.8, and 23.9 nm for samples S1, S2, and S3, respectively.

TEM images show that the products S2 and S3 prepared with current solvothermal post-treatment have ordered mesostructures. The ordered domains can be extended to several micrometers, indicating that solvothermal treatment does not deteriorate the structural regularity of the mesostructured membranes. Figure 2, parts a and b, shows TEM images of S2 taken with [111] and [311] incidences, respectively, of *Ia*-3*d* space group, with cell parameter *a* of 19.6 nm that is in agreement with the value calculated from XRD patterns. From the Fourier diffractograms (FD) (see figures for detailed indexations), the space group (in domains) is uniquely determined to be *Ia*-3*d*, which is the same as that for MCM-48 and FDU-5,[10] further corroborating the conclusion derived from XRD patterns. It should be noted here that the gyroidal mesoporous silica materials prepared herein exhibit certain structural distortion; hence the considerable loss of symmetry in certain domains. This can be clearly seen in the TEM images of [111] and [531] incidences (Figure 2, parts c and d, respectively). Therein the arrows clearly indicate the contraction along ⟨211⟩ direction. As a result, the original three-fold axis along [111] incidence (six-fold in projection) disappears and reduces to the two-fold axis of the rectangular patterns, and the [01−3] and [2−3−1] vectors are not perpendicular with respect to each other in [531] incidence anymore. The proposed explanations for this unidirectional shrinkage may be as follows: The gyroidal mesostructure is transformed from the 2D hexagonal rudimentary form. And quite similar to previous literature,[23] the 2D hexagonal mesostructures are contracted and can be described as a 2D-centered rectangular mesophase (*c*2*m*) in domains. Therefore after phase transition, the gyroidal mesostructure retains the inherited orientational distorted portions, assuming the phase transition process does not significantly disarrange the mesoscopic networks. From the TEM analysis shown above, we can make two speculations. (a) Since the contraction direction of the membrane "precursor" (2D hexagonal) and the post-solvothermally treated "product" (3D cubic) should be the same, the [10] direction of the former corresponds to the [211] direction of the latter mesostructure. This fact further corroborates the hypothesis that there is a geometric correlation between the [10] planes of the 2D hexagonal and the [211] planes of the 3D gyroidal mesophase, or that the cylinder axis of the 2D hexagonal phase equals the body diagonal ([111] direction) of the gyroidal cubic phase. (b) If the mesophase transition induced by the solvothermal post-treatment was applied to prepare double gyroidal mesoporous silica thin films deposited on a substrate (e.g., silicon wafer), the channel networks of the gyroidal mesostructured thin films would orient with one [111] axis parallel along the substrate. Accordingly, the top surface of the thin films would correspond to the penetrable (211) mesoscopic planes.

Another type of structural distortion may also be directly originated from the imperfection of the 2D silica membrane "precursors". Different from distortion caused by the uniaxial shrinkage in the direction normal to the substrate, it is generated parallel with the substrate. Because of the inevitably curved nature of the channel direction of the 2D hexagonal domains,[23] the (111) planes of transformed gyroidal mesostructure may actually pack tortuously along the curved [111] direction, hence inducing the distortion of other related planes. Moreover, some severe structural mismatch or dislocation (only a very small fraction) may hinder the successful structural transformation. Figure 3 shows the TEM image of mesoporous silica product (S2) viewed along [531] incidence, in which incomplete transformation can be observed. The branched and curved paintbrush-like channels[25] of the 2D hexagonal mesophase are preserved since its channel axis is highly distorted (see the dotted arrow), which inhibits the phase transition. All the structural imperfection analyzed above should be responsible for the less resolved Bragg diffraction peaks in XRD patterns. It should also

(24) (a) Landry, C. C.; Tolbert, S. H.; Gallis, K. W.; Monnier, A.; Stucky, G. D.; Norby, P.; Hanson, J. C. *Chem. Mater.* **2001**, *13*, 1600. (b) Gallis, K. W.; Landry, C. C. *Chem. Mater.* **1997**, *9*, 2035.

(25) Zhou, W.; Ma, X. C.; Yuan, Z. Y.; Wang, E. G. *Surf. Interface Anal.* **2001**, *32*, 236.

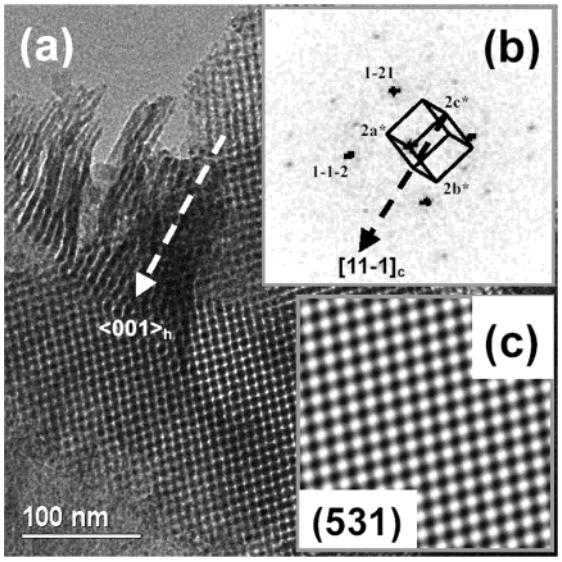

Figure 3. TEM image of calcined gyroidal mesoporous silica (S2), (a) viewed from [531] direction, (b) its FD picture, (c) and TEM simulation. The (531) projection of *Ia*-3*d* cubic reciprocal cell is superimposed on the FD picture. The dashed arrows in (a) and (b) show the alignment of ⟨001⟩ vectors for 2D hexagonal and the [11−1] vectors for 3D cubic mesophases.

be noted that, as seen in Figure 3, the mutual alignment of channel direction of 2D hexagonal and $[11-1]_c$ (c is denoted as cubic mesophases) is perfect. The vector $[11-1]_c$ is not parallel to (531) plane; it is tilted, and channel direction of 2D hexagonal is also tilted from the corresponding plane, as shown in Figure 3b. The correlation between the paintbrush-like channel direction and $\langle 111\rangle_c$ further confirms that the cylinder axis of the hexagonal phase transforms to the body diagonal direction of the gyroidal phase.

This novel method can be extended to the preparation of other silica-based mesoporous materials with gyroidal structures (see details in the Supporting Information). For example, metal (nonmetal) ions doped (such as Ti, Al, W, Nb, Mn, B, etc.) bicontinuous cubic mesoporous silica can be similarly prepared by co-condensation of TEOS with alkoxides or metal chlorides containing various inorganic heteroatoms during EISA, followed by solvothermal treatment and direct calcination. XRD patterns and TEM images show the metal (nonmetal) ions doped mesoporous silica materials have ordered bicontinuous cubic mesostructure comparable to that of pure silica mesoporous materials. The doping ratio [metal (nometal)/Si molar ratio] can reach to 1/8 while keeping the regularity of the mesostructures. Hybrid organo-functionalized ordered cubic (*Ia*-3*d*) mesoporous silica materials can also be synthesized by solvothermal post-treatment, using various $RSi(OEt)_3$ or $RSi(OMe)_3$ (e.g., R = 3-aminopropyl, 2-mercaptopropyl, 3-chloropropyl, etc.) as the dopants and employing tetrahydrofuran to extract the organic templates. The $RSi(OEt)_3$ or $RSi(OMe)_3$ can be mixed up to 5% (molar ratio), and the structural regularities determined by XRD patterns only slightly deteriorate with the increase of the doping ratio.

We sketch a simplified schematic diagram to help visualize the possible structural correlation between the 2D hexagonal and 3D bicontinuous cubic mesostructures. The rudimentary and final channel structures viewed from $[10]_h$ and $[211]_c$ directions are shown in Scheme 1, parts a and c, respectively, considering the fact that the cylinder axis (paralleled to the (10) plane) of the hexagonal phase is equivalent to the body diagonal (paralleled to the (211) plane) of the gyroidal cubic phase.[24a,26] Each channel is labeled as A, B, or C. For the 2D hexagonal mesostructure, the channels A, B, and C are equal with respect to each other and align side by side (the interdistance is the cell parameter, *a*, of the 2D hexagonal phase). An intermediate state (Scheme 1b) caused by the thermal-induced framework rearrangement, assumes that channel B begins contacting channel A and C at equidistant sites (note the adjacent A and C channels are always separate). A final form, i.e., 3D bicontinuous cubic mesostructure, is achieved by uniformly dividing channel B and merging totally with channels A and C at the contacting sites, accompanying the curvature change. The bicontinuous channels (A and C) are aligned along the [0−11] direction, and the single channel is extended along the [1−1−1] direction. An interval of $2d_{(0-11)}$ is calculated between adjacent equal (A or C) channels on this projection plane. It should be noted that the same channels (A or C) connect as a whole at periodic positions above and beneath this hypothetic plane, producing gigantic bicontinuous networks. The simulated perspective model of interwoven channels (Scheme 1d) gives a further 3D insight into the planar structures shown in Scheme 1c and analyzed above. The double channels are marked by light green and pink, respectively. At the A or C sites and parallel with the [1−1−1] axis (namely, the body diagonal direction, not shown here), only a light green channel or pink channel is observed, indicating the extension of a single continuous channel along this direction, whereas at B sites and along the same direction, pink and light green channels appear alternately and link with adjacent channels (A or C).

The phase transition from *p*6*mm* to *Ia*-3*d* has been successfully investigated for the MCM-41/MCM-48 systems,[24] and proper alkaline conditions as well as surfactant concentration should be considered. In that case, the inorganic region of the mesostructure is sufficiently unpolymerized that surfactant-packing considerations controlling rearrangements in the organic region of the mesostructrue can be used to manipulate the ultimate pore geometries. Previous work has proved futile to prepare MCM-48-related materials via phase transition under an acidic condition, probably due to the irreversible siliceous hydrolysis/condensation nature therein (acidic condition). Then, why are our large-pore bicontinuous mesoporous materials successfully prepared via the phase transition from 2D hexagonal structure under acidic conditions and why not using as-made highly ordered SBA-15 powder as the starting "precursors"?

Peaks assigned to Q^2 (−90.2 ppm), Q^3 (−99.57 ppm), and Q^4 (−107.78 ppm) can be clearly distinguished in the ^{29}Si MAS NMR spectrum of product S5 (as-made silica membrane prepared by EISA and using *P*123 as a template) (see Supporting Information). Since the Q^2 and Q^3 signals are indicative of the existence of incompletely polymerized silica species and the calculated $(Q^2 + Q^3)/Q^4$ ratio of the as-made hybrid silica membrane S5 is 2.43 (the value of the calcined membrane S1 is around 0.21), very low degree of silica polymerization or good flexibility of the frameworks can be concluded. In contrast, the as-made SBA-15 powder, prepared under hydrothermal condition at 40 °C and without further high-temperature heating treatment, shows relatively weaker Q^2 and Q^3 signals, and the

(26) (a) Rancon, Y.; Charvolin, J. *J. Phys. Chem.* **1988**, *92*, 2646. (b) Clerc, M.; Levelut, A. M.; Sadoc, J. F. *J. Phys. II* **1991**, *1*, 1263.

Scheme 1. Possible Phase Transition Model from *p6mm* to *Ia-3d*[a]

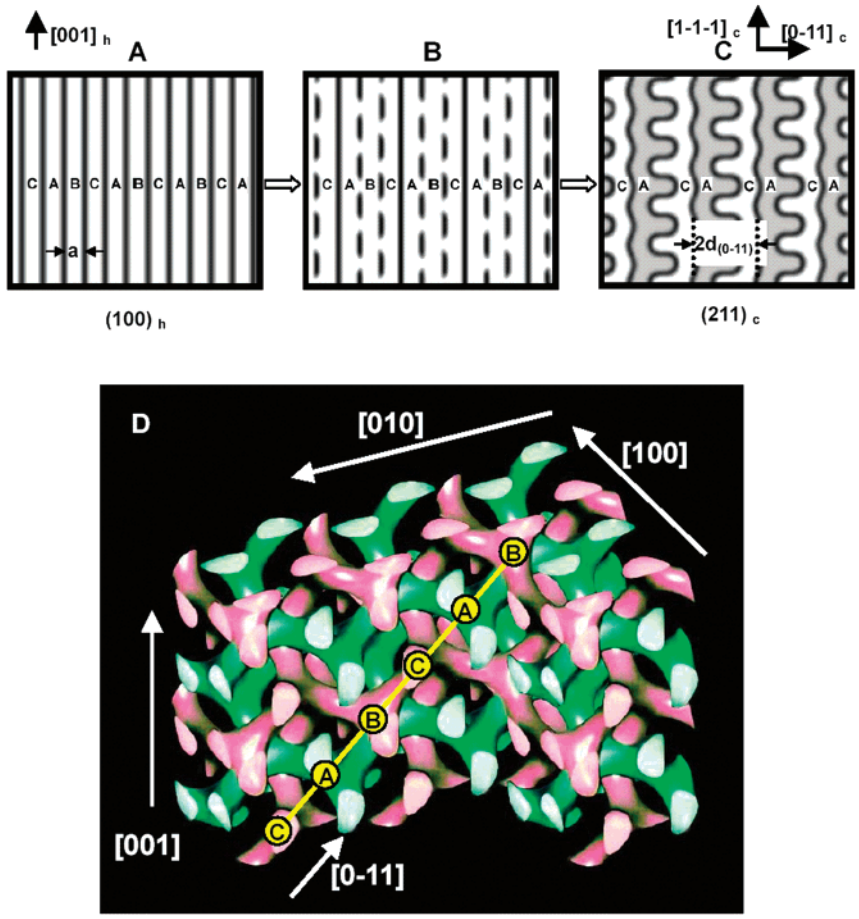

[a] (A) (100) Plane of 2D hexagonal phase, (B) an intermediate phase, (C) (211) plane of cubic gyroidal phase, and (D) 3D model of double gyroidal channel structures.

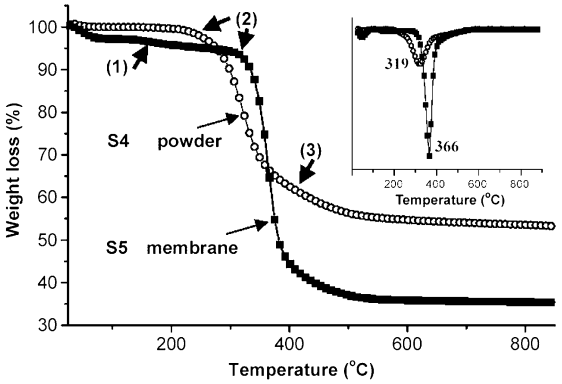

Figure 4. TGA and DTG (inset) curves of as-made SBA-15 powder (S4) and as-made silica membrane (S5).

value of $(Q^2 + Q^3)/Q^4$ ratio is 1.24. Therefore, it is apparent that it is easier for as-made silica membranes prepared from EISA to undergo structural rearrangement than for the SBA-15 powder, though both of them are templated by triblock copolymer Pluronic P123. This is unambiguously because of the nearly "nonaqueous" solvent (ethanol) used for the preparation of hybrid silica membrane, whose inert nature impedes the silica condensation.

Thermogravimetric analysis (Figure 4) clearly shows that the content of the organic species (*P*123) of the hybrid silica membranes (such as S5) is around 61 wt % (having subtracted the weight loss caused by absorbed water), much higher than that of as-made SBA-15 powders (ca. 45 wt %). Combined with the fact that the current hybrid membrane S5 and SBA-15 powders are all templated by block copolymer Pluronic *P*123 and the copolymer/TEOS ratios (mass ratio, 1:2.08) are equal in both mother solutions, we conclude that only part of block copolymers participate in the self-assembly synthesis of SBA-15 powder while nearly 100% participate in the membrane S5.[27] It has long been accepted that MCM-48-related materials were always synthesized at higher concentrations of single mesoscopic structure-directing agent than for MCM-41. In the current case, the membrane "precursors" contain more block copolymers whose mesophase may undergo curvature change more readily upon heating and, hence, the easier phase transition to form gyroidal mesostructure.

Furthermore, we observe that in the temperature range of 130−230 °C, the as-made membrane sample (S5) shows noticeable weight loss (see arrow 1), which is partially due to the condensation process of the unpolymerized silica species, corroborating the MAS NMR results that the as-made silica membrane has a low degree of framework cross-linkage. More importantly, the onset temperature (see arrow 2) for the decomposition of the organic templates in the membrane sample lags behind that in the SBA-15 powder sample by nearly 80 °C, suggesting that the block copolymers are loosely packed

(27) Assuming all TEOS are transformed to SiO_2 and no loss of *P*123, the theoretical weight loss of block copolymer upon thermal decomposition should be $1/(1 + 0.6) = 62.5\%$.

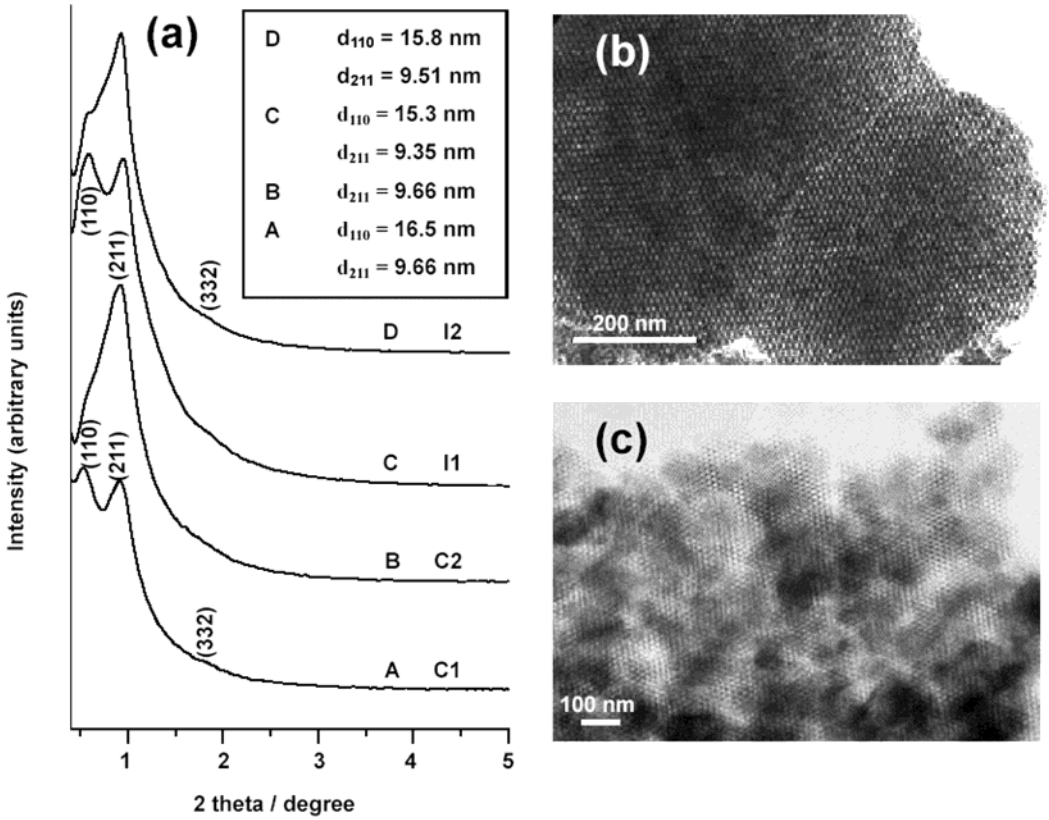

Figure 5. Small-angle XRD patterns (a) and TEM images (b and c) of Co_3O_4 and In_2O_3 replicas templated by microwave-digested gyroidal mesoporous silica (sample S3).

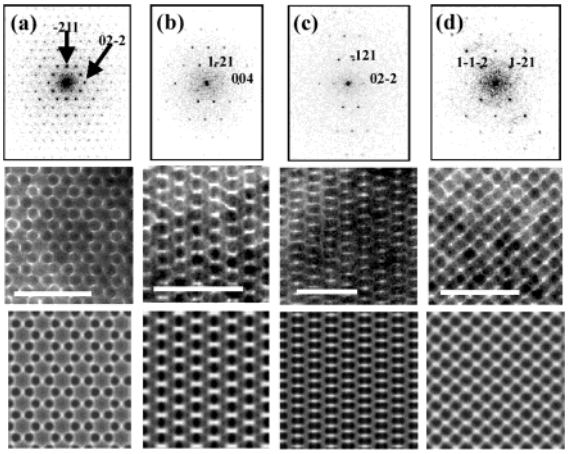

Figure 6. Fourier diffractograms (top), fragments of TEM images (middle) and TEM image simulations (bottom) of the mesostructured replicas (a) In_2O_3 along the [111], (b) Co_3O_4 along the [210], (c) In_2O_3 along the [311], and (d) Co_3O_4 along the [531] directions. Scale bar is 50 nm.

(air may access the channels more easily) for SBA-15 powder. However, the decomposition rate of *P*123 for the membrane is much greater than that for the SBA-15 powder, as can be seen in the differential thermogravimetric (DTG) curves in the inset of Figure 4, and a relatively larger tail during the whole decomposition process of the SBA-15 powder can be observed (arrow 3). The above facts may be suggestive of the degree of insertion of PEO moieties within the silica walls, and it may be concluded that there are much fewer PEO moieties inserted into the inorganic matrix for the as-made membrane. N_2 sorption measurements further support this conclusion (see below). The inclusion of PEO segments is deleterious to the mesophase transition because of the much reduced mobility of the organic templates. Previously documented phase transitions from 2D hexagonal to 3D bicontinuous cubic all consider the simple cationic surfactants, whose headgroups never penetrate into the inorganic walls.

It has been established that the micropores of mesoporous materials are partially caused by the inserted PEO corona in the as-made products.[28] N_2 sorption data (see Supporting Information) show that the calcined 2D hexagonal membrane (S1) has very low micropore volume (V_{mi}) and micropore area (S_{mi}), which further suggests the conclusion that nearly no PEO segments penetrate into the silica walls. The $W_{BJH}S_p/V_p$ value (S_p, mesopore area, V_p, mesopore volume; they are replaced by S_{BET} and V_t herein) of S1 is calculated to be 4.15,[28] further suggesting that the nonmicroporous nature and the perfect tubular channels of the calcined mesoporous silica werepreparedvia the EISA process. The micropores are also negligible in S2, a calcined gyroidal mesoporous silica.

In sum, the good flexibility of the silica framework makes possible the acidic phase transformation from 2D hexagonal to 3D bicontinuous cubic; this good flexibility (or low degree of silica condensation), high content and tight packing of organic amphiphilic molecules, and great mobility of organic templates

(28) (a) Kruk, M.; Jaroniec, M.; Ko, C. H.; Ryoo, R. *Chem. Mater.* **2000**, *12*, 1961. (b) Ryoo, R.; Ko, C. H.; Kruk, M.; Antochshuk, V.; Jaroniec, M. *J. Phys. Chem. B* **2000**, *104*, 11465. (c) Ravikovitch, P. I.; Neimark, A. V. *J. Phys. Chem. B* **2001**, *105*, 6817. (d) Imperor-Clerc, M.; Davidson, P.; Davidson, A. *J. Am. Chem. Soc.* **2000**, *122*, 11925. (e) Galarneau, A.; Cambon, H.; Di Renzo, F.; Fajula, F. *Langmuir* **2001**, *17*, 8328. (f) Joo, S. H.; Ryoo, R.; Kruk, M.; Jaroniec, M. *J. Phys. Chem. B* **2002**, *106*, 4640. (g) Galarneau, A.; Cambon, N.; Di Renzo, F.; Ryoo, R.; Choi, M.; Fajula, F. *New J. Chem.* **2003**, *27*, 73.

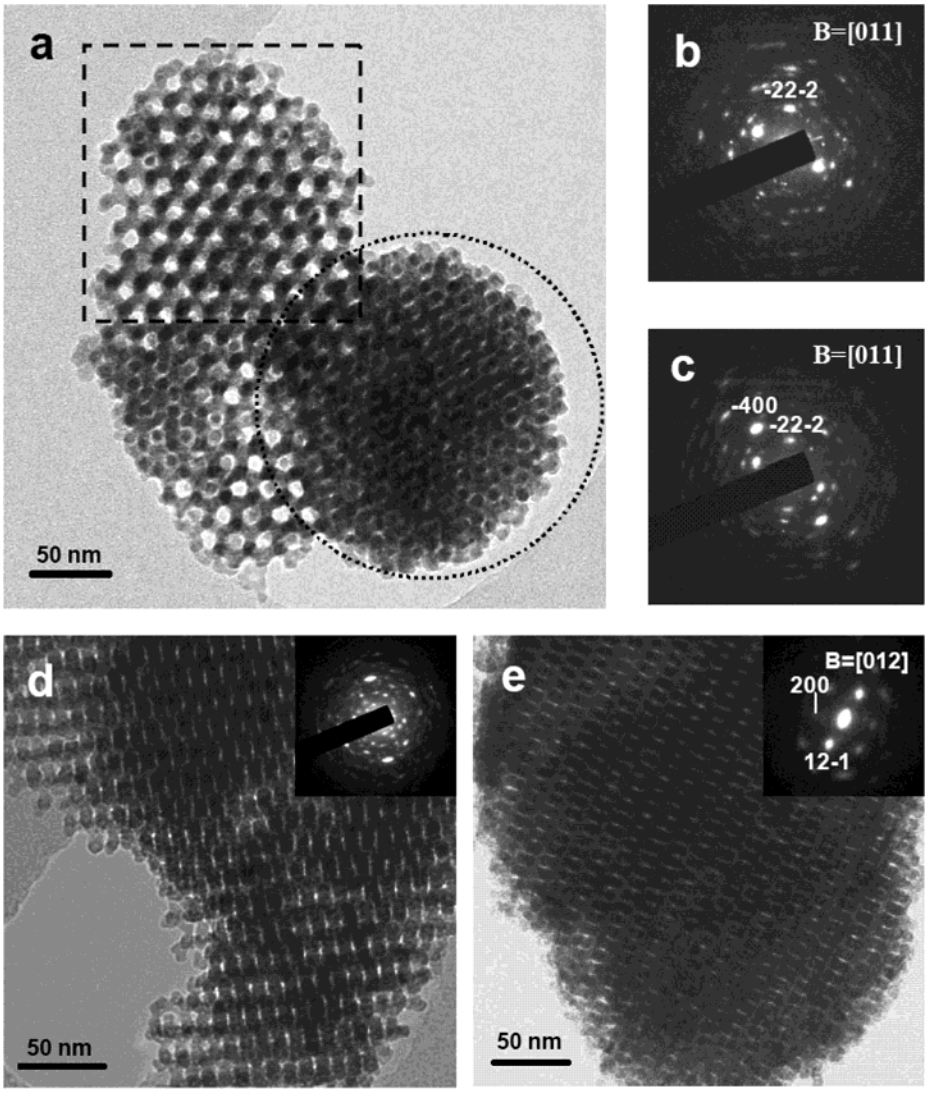

Figure 7. TEM images (a, d, and e) and corresponding SAEDs (b, c and insets in d and e) of In_2O_3 replica, viewed from [111] (a) and [311] (d and e) mesoscopic directions. (a and e) Sample I2; (d) sample I1.

may also explain why current as-made silica membranes can undergo structure rearrangement while as-made SBA-15 powder may not.

The employment of hexane (results show that other medium or long-chain alkanes also work, e.g., heptane, octane, paraffin) instead of water as the heating media plays a decisive role in the formation of gyroid cubic mesophase. Different from water that can greatly facilitate the hydrolysis and condensation of siliceous species and improve the regularity of 2D hexagonal mesostrutures, hexane is more inert as to the reaction with inorganic siliceous species; therefore, it may basically transfer energy to trigger the mesophase transition at the early stage. Upon being heated (80 °C), the hydrophobicity of the amphiphiles increases, resulting in the increased assembly parameter of the surfactant[29] or decreased interface curvature, which leads to the phase transition from 2D hexagonal (*p*6*mm*) to bicontinuous cubic (*Ia*-3*d*). Preliminary XRD data (see Supporting Information) show that phase transition occurs just in the first half hour of solvothermal treatment. However, the framework rigidity, indicated by ^{29}Si NMR spectra, increases very slowly, and several days of solvothermal treatment are required to match that obtained by only 1 h of hydrothermal treatment. Therefore, we believe that the solvothermal treatment has well-controlled thermodynamic and kinetic behaviors, i.e., separate the competing stages of phase transition and structure freezing apart, which pave the successful synthesis of large-pore gyroidal mesoporous materials under acidic condition.

2. Mesorelief Metal Oxides. Until now, nonsiliceous mesostructured materials were usually prepared by the supramolecular templating strategy, the same as in the case of silica. However, this "general" method has many restrictions that impede some future applications.[1a,2c] An alternative approach addressing the above problems is developing, i.e., employ ordered hard mesoporous templates to mold the "negative" ordered mesorelief objects. Here, the prepared 3D double gyroidal mesoporous silica can further serve as the hard templates for the preparation of various mesorelief metal oxide materials. Compared with calcined bicontinuous cubic mesoporous silica materials (S2), microwave-digested mesoporous silica sample (S3) exhibits higher surface area and silanol population, larger pore size and pore volume, and more importantly, the existence of micro/(meso)pore connections[30]

(29) Namely g, $g = v/la_0$, where v is the hydrophobic chain volume, l is the chain length, and a_0 is the effective optimal surface.

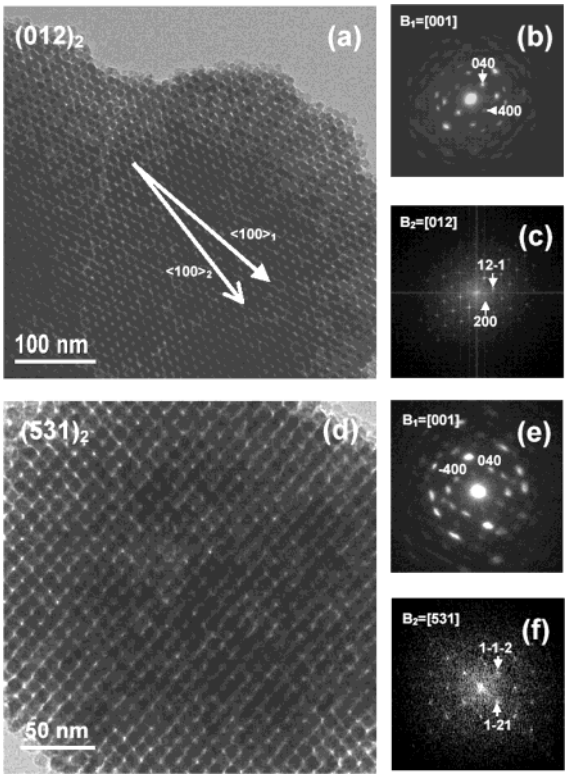

Figure 8. TEM images, SAEDs, and FDs of Co_3O_4 mesorelief materials (C2).

between the double gyroidal channels (see Table 1 of the Supporting Information). Therefore, we chose the digested materials (S3) as the sacrificial "molds" and employed simple impregnation and thermolysis procedures to prepare the "negative" ordered mesorelief metal oxides.

Figure 5a shows the small-angle XRD patterns for Co_3O_4 and In_2O_3 gyroidal porous crystals prepared by using mesoporous silica (S3) as a template after the removal of silica frameworks. C1 and I1 were prepared with less hydrated metal nitrate precursors while C2 and I2 were prepared with more. Accordingly, C1 and I1 exhibit two broad Bragg diffraction peaks at 2 θ values below 1°, which can be indexed to 110 and 211, respectively. However, C2 and I2 show basically one diffraction peak, roughly indexed to the 211 diffraction. It is known that the extinction of 110 corresponds to the dominance of undisplaced double gyroidal frameworks (space group, *Ia*-3*d*), while its appearance is suggestive of the existence of a large fraction of displaced or uncoupled subframeworks (space group, $I4_132$ or lower).[7c,17a,22a] Therefore, it may be concluded that the ratio of undisplaced/(displaced + uncoupled) enantiomeric gyroidal (sub)frameworks can be tuned just by changing the infiltration amount of metal nitrate precursors. The results suggest that within a certain synthetic range, the more inorganic precursors used, the more efficient and faithful the replication procedures. The second step impregnation not only increases the total filling amount, but also helps mend the structural defects of metal oxide replicas and further copies the structural details (especially the self-supporting connections derived from the micro- or mesotunnels on the mesopore walls) of the silica molds. The wide-angle XRD patterns of these metal oxide replicas exhibit broadened Bragg diffraction peaks (see Supporting Information), suggesting that these metal oxides are readily crystallized within the confined nanospace. The In_2O_3 and Co_3O_4 mesorelief materials are evidenced as body-centered cubic (a = 10.118 Å, *Ia*-3, JCPDS: 06 416) and face-centered cubic (a = 8.084 Å, *Fd*-3*m*, JCPDS: 421 467) phases. The relative intensities of various peaks match well with the bulk metal oxides, suggesting the isotropic crystallization nature of the replicas. The average thickness of a single strand of gyroidal crystals is calculated by the Scherrer equation to be 9.50 ± 0.05 and 13.3 ± 0.05 nm for In_2O_3 (I_2) and Co_3O_4 (C_2), respectively.

Figure 5, parts b and c, shows the typical TEM images of Co_3O_4 and In_2O_3 replicas. Long-range ordering (extended to several micrometers) can be observed, suggesting the efficient infiltration of metal oxide precursors, which is in accord with the SEM results that the particle size is larger than 500 nm on average. EDX data confirm the nearly complete removal of silica from the replicas, hence, the self-supported nature of the gyroidal metal oxide crystals. The ease of "guest" materials replication clearly results from the unique 3D open channels of the "host" materials and the microwave digestion treatment used herein. A single double gyroidal mesostructured silica particle has abundant isotropic pore entrances but only two channels, hence very high probability of importing "guest" materials in one continuous channel. Microwave digestion treatment, as previously suggested, optimizes this process by enhancing the "host−guest interaction" (by preserving the dense silanol groups whose hydrophilic nature helps to attract hydrated metal nitrates) by increasing the accommodating capacity (by enlarging the pore size, pore volume, etc.) and by generating framework "joints and bolsters" (by creating micro- and mesopore connections).

Characteristic TEM images of the inverse metal oxide materials (Figure 6) are shown in comparison with respective TEM simulations. The images correspond well with the model of a self-supported bicontinuous framework material replicating the pore system of cubic mesoporous template with *Ia*-3*d* symmetry. The FDs of the TEM images indicate long-range mesostructure ordering, though the angles (Figure 6c) between the diffraction vectors deviate noticeably from those expected for cubic symmetry. The latter evidences a distortion of the mesostructure lattice, which, in turn, explains the poor resolution of the low-angle X-ray powder diffractograms of the materials (Figure 5a). The framework distortion of replicated metal oxides very likely results from the distorted "molds" as detailed above.

Three typical domains, undisplaced frameworks (UD), displaced frameworks (DP), and uncoupled subframework (UC) can be clearly observed for incompletely replicated samples (I1 or C1). TEM images of three type of domains, simulations of UD and DP, and the model of UC are shown in Figure 6 of the Supporting Information. The structure of the oxide frameworks formed within the pores of the silica templates may be considered as built of conjugate trefoil fragments formed by roughly cylindrical segments. It should be noted again that the triblock copolymers will render the micropores and mesopores sprinkled onto the silica mesopore walls, paving the possibility of faithful structural transcription upon the mold removal.

(30) We propose a possible explanation for the existence of micro/(meso) pores: microwave digestion (MWD) is unique in that a strong acidic (HNO_3) and oxidative (H_2O_2 + HNO_3) system is used. The MWD is carried out under high pressure (above 10 atm) and microwave irradiation. Therefore, the siliceous framework may undergo local structural evolution, e.g., rehydrolysis and recondensation, and the micropores and/or mesopores can form and locate within the mesopore walls during this short digestion period (within 10 min).

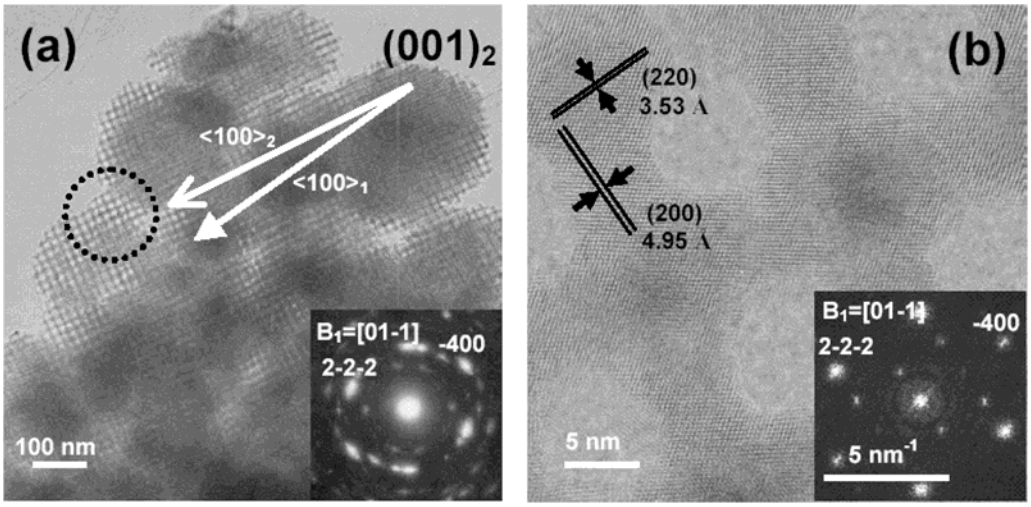

Figure 9. TEM image (a), SAED (inset of a), HRTEM image (b, circular domain of a), and FD (inset of b) of In_2O_3 mesorelief material (I1).

Therefore, UDs can be transcribed from the triblock copolymer-templated double gyroidal mesoporous materials, which is in contrast to CMK-1.[16a] As to DP and UC domains, it is obviously caused by the immature structural transcription due to the lack of inorganic "nutrients". And accordingly, two subframeworks displace with respect to each other (DP), or just remain single (UC), after the silica molds were etched away. TEM images of sample I1 show large UC domains and corroborate well the XRD curve (C) shown in Figure 5a; therein 110 diffraction is evident. The mean diameter of the cylindrical oxide framework segments is 8 nm, which was estimated by analyzing the TEM image fragments showing individual uncoupled subframeworks. For proper averaging, the inverse Fourier transform mask filtering is applied to the measured image fragments. TEM images of the samples I2 and C2 prepared with more inorganic precursors show a much larger fraction of UD domains, further suggesting the possibility of framework "engineering".

The single crystallinities of the gyroidal metal oxides are further characterized by selected area electron diffraction (SAED) patterns. Figure 7a shows the TEM image of a small fragment of In_2O_3 replica (sample I2), which is viewed from [111] zone axis. The square and circular domains are indicative of single uncoupled subframework and coupled frameworks, and their SAED patterns shown in Figure 7b,c can be indexed to [011] incidence of cubic In_2O_3, but clearly the square domain exhibits much poorer single crystallinity. This fact suggests that incomplete infiltration may give rise to incoherent crystallites formation and, hence, a poor-resolved SAED pattern. This tentative idea is further confirmed by the images shown in Figure 7, parts d and e, which correspond to the displaced and undisplaced (311) mesoscopic projections of I1 and I2, respectively. The SAED pattern of I1 (Figure 7d, inset) is hard to index while that of I2 (Figure 7e, inset) can be well indexed to be the [012] incidence of In_2O_3 crystals. Therefore, it can be concluded that the single crystallinity of the gyroidal metal oxide replica particles greatly depends on the amount of the inorganic precursors used for the following two reasons. First, insufficient precursors tend to deplete more readily upon thermolysis, hence leaving a large fraction of vacancies within the silica channels, which is disadvantageous for the formation of large single crystals. Second, insufficient precursors are limited to produce undisplaced frameworks (self-supported frameworks) since their access to the channel connections (within the silica walls) is very challenging and they are unable to further mend the structural imperfections. Therefore, the undisplaced frameworks usually show higher degree of single crystallinity (Figure 7a, circular domain and Figure 7e), and the contrary for the displaced (Figure 7d) or uncoupled domains (the rectangular domain of Figure 7a and the margin of Figure 7d).

The correlation of double scale orderings of the replicated metal oxide porous crystals can be clarified by (HR)TEM, SAED (camera length, 20 cm), and FDs, as shown in Figures 8 and 9. The SAED (Figure 8b) of the corresponding Co_3O_4 replica (sample C2, TEM image shown in Figure 8a) shows the single crystalline nature of the gyroidal metal oxide frameworks. Furthermore, it can be derived that the electron incident beam is along the [001] atomic zone axis of the cubic Co_3O_4 crystals. The relevant $\langle 100\rangle_1$ (the subscript 1 and 2 denote the atomic and mesoscopic scales, respectively.) crystallographic direction is shown as a white arrow in Figure 8a, compared with the $\langle 100\rangle_2$ mesoscopic direction calculated from the FD (Figure 8c) of the same TEM image. This mismatch suggests that the idea of the most possible double scale correlation, $\langle 100\rangle_1$ parallel with $\langle 100\rangle_2$, is untenable. But it still cannot exclude the possibility of other structural correlations since $[001]_1$ is right paralleled with $[012]_2$ direction at the current projection. Figure 8d shows the (531) mesoscopic projection plane of gyroidal structure, and its SAED (Figure 8e) can be also assumed as (001) plane of Co_3O_4 crystal. Considering the beam directions in Figure 8, parts b, c, e, and f, and the fact that $\langle 210\rangle$ is not parallel or perpendicular to $\langle 531\rangle$, we are safe to say that there is no structural correlation between the mesoscopic and the atomic orderings. TEM/SAED and HRTEM/FD of In_2O_3 replica (sample I1) after removing the silica template are shown in Figure 9, parts a and b, respectively. Combined with the HRTEM ((200) and (220) lattice spacings) and FD, the SAED projection can be indexed to be {110} crystallographic plane (note, for comparison purpose, that we assume the beam direction is [01−1]). The corresponding $\langle 100\rangle_1$ and the nearest $\langle 100\rangle_2$ directions shown in Figure 9a do not parallel with each other, either. This fact also suggests the mismatch of the most possible correlated double scale orientations. Combined with other detailed characterizations, the double scale orders of the In_2O_3 replica are not commensurate with each other, either. We

tentatively propose the following possible explanations for the noncorrelation behavior between these two scales. First, both Co_3O_4 and In_2O_3 are crystallographically isotropic (face-centered cubic or body-centered cubic). This nature facilitates the "guest" replication, especially of the structural details, probably due to the kinetic equality of crystal growth (filling and mending). Unfortunately, the isotropic properties also make the crystal growth random within the specific mesopore domains. Second, the framework of the silica "host" is highly curved, i.e., there is no straight orientations. Moreover, the "host" is also structural isotropic (3D cubic) compared with the 2D hexagonal mesostructure. Therefore, the directional and dimensional restrictions exerted by the "host" seems meaningless, which leads to nonpreferential growth of oxide crystals. Third, there is no special structural matching at the interface between the "host" and "guest" materials, that is, the amorphous silica cannot guide the nucleation and epitaxial growth of the metal oxide crystals. Finally, the silica "mold" is distorted in domains, dampening the possibility of consistent transcriptions.

The optical properties of nanostructured metal oxide porous crystals are further characterized by UV−DRS and room-temperature photoluminescence (PL) spectroscopy (see Supporting Information). UV−DRS spectra of the mesorelief In_2O_3 sample I1 show a strong absorption peak centered at around 300 nm, which is blue-shifted by about 35 nm compared with the bulk In_2O_3 (sample I3), suggesting the possible quantum confinement effect. At least two broad emission bands centered at 477 and 544 nm (typical of the nanoscaled In_2O_3 materials[31]) can be observed for sample I1, in contrast to the much weaker PL spectrum of sample I3. These peaks are probably resulted from the oxygen vacancies located at the In_2O_3 gyroidal surface[31] generated during the annealing process. The complexity of the gyroidal structures and other framework characteristics may also contribute to the observed PL behavior, which are currently under study.

Besides Co_3O_4 and In_2O_3 detailed here, the current impregnation and thermolysis procedures can be generally extended to the preparation of other mesorelief metal oxide composites, such as Cr_2O_3, NiO, Fe_2O_3, Mn_xO_y, CeO_2, WO_3, etc., by using corresponding hydrated metal nitrates or polyacids as the inorganic precursors. These nanostructured metal oxides generally have BET surface areas above 70 m^2/g, pore volumes above 0.15 cm^3/g, and narrow mesopore size distributions that are derived from the ordered inorganic framework voids.

(31) (a) Zhou, H. J.; Cai, W. P.; Zhang, L. D. *Appl. Phys. Lett.* **1999**, *75*, 495. (b) Zhang, J.; Qing, X.; Jiang, F. H.; Dai, Z. H. *Chem. Phys. Lett.* **2003**, *371*, 311.

Conclusions

Ordered large-pore double gyroidal (*Ia*-3*d*) mesoporous silica-based materials have been effectively synthesized utilizing a new post-solvothermal procedure. The low polymerization of inorganic framework, relatively high content, and flexible nature of organic matrix are the preconditions of mesophase transition from 2D hexagonal to 3D bicontinuous cubic, which is later triggered by the nonaqueous heating media. A phase transition model is proposed to address the structural evolution from the rudimentary to the final forms, and the mesoscopic distortions are discussed in detail. Micrometer-scaled nanoporous metal oxide crystals, such as Co_3O_4, In_2O_3, Cr_2O_3, NiO, Fe_2O_3, Mn_xO_y, CeO_2, and WO_3 etc., are for the first time generally transcribed from the titled mesoporous silica via simple impregnation and thermolysis procedures. Their single crystallinities depend highly on the amount of precursors used. The metal oxide crystals show double scale orderings, but no specific orientations have been observed. The hierarchically ordered single crystalline metal oxides are important both for the systematic fundamental study of structure−property relations and for their technological promise in applications such as catalysis, sensor arrays, battery and bioactive materials, miniaturized devices, and beyond.

Acknowledgment. This work was supported by NSF of China (Grant Nos. 29925309, 20233030, and 20173012), Shanghai Nanotech Promotion Center (0212nm043), Shanghai Science & Technology Committee (03DJ14004, 02ZA14005), State Key Basic Research Program of PRC (2002AA321010, 2001CB610506), the grants of INTAS 01-2283, KRSF-RFBR 02-03-97704, and RFBR 03-03032127. We thank Qinghai Song, Lei Xu, Liying Liu, Qihui Shi, Jian Yang, Ying Chen, and Huiwen Jiang for experimental and charaterization assistance.

Supporting Information Available: Detailed materials syntheses, XRD patterns of silica materials, TEM images of boron-doped and 3-chloropropyl-functionalized gyroidal mesoporous silica-based materials, N_2 sorption isotherm curves, table of N_2 sorption data, NMR spectra of hybrid materials, scheme of 2D channel structures, wide-angle XRD patterns of I_2 and C_2, additional TEM images of In_2O_3 replicas, and UV−vis and PL spectra of In_2O_3 materials (PDF). This material is available free of charge via the Internet at http://pubs.acs.org.

JA037877T